Hindawi
Adsorption Science & Technology
Volume 2022, Article ID 7385541, 16 pages
https://doi.org/10.1155/2022/7385541

Research Article

A Study of Methylene Blue Dye Interaction and Adsorption by Monolayer Graphene Oxide

Jakub Ederer,[1] **Petra Ecorchard**,[2] **Michaela Šrámová Slušná**,[2] **Jakub Tolasz**,[2] **Darina Smržová**,[2] **Simona Lupínková**,[3] **and Pavel Janoš**[1]

[1]*Faculty of Environment, University of Jan Evangelista Purkyně, Pasteurova 3632/15, 400 96 Ústí nad Labem, Czech Republic*
[2]*Institute of Inorganic Chemistry of the Czech Academy of Sciences, 250 68 Husinec-Řež, Czech Republic*
[3]*Faculty of Science, University of Jan Evangelista Purkyně, Pasteurova 3632/15, 400 96 Ústí nad Labem, Czech Republic*

Correspondence should be addressed to Jakub Ederer; jakub.ederer@ujep.cz

Received 25 April 2022; Revised 15 July 2022; Accepted 20 July 2022; Published 9 August 2022

Academic Editor: Muhammad Raziq Rahimi Kooh

The graphene oxide (GO) interaction with methylene blue (MB) cationic dye was studied in an aqueous solution at different pH during MB adsorption. The mutual interaction of MB with GO surface was studied and evaluated by Fourier transform infrared spectroscopy (FTIR) and X-ray diffraction (XRD). The π-π and electrostatic interaction of MB with GO surface are the main types of interactions, and the XRD data show the monomeric arrangement of MB cation with GO. The GO surface functional groups and point of zero charge (PZC) were determined by acid-base titration. Suitability of zeta-potential measurement and acid-base titration method was briefly discussed. The quality of prepared GO was evaluated by Raman spectroscopy, XRD, and atomic force microscope (AFM). The experimental adsorption equilibrium data were analyzed using Langmuir, Langmuir-Freundlich, Freundlich, and Temkin isotherms. The GO maximum adsorption capacity increases with higher pH, that is ascribed to the facile interaction of negatively charged GO with positively charged MB structure.

1. Introduction

The growth of the textile industry is responsible for the increasing pollution, mainly in the water environment. The textile industry commonly uses plenty of dyes, representing potential dangers for nature and health [1]. Moreover, many dyes are toxic and carcinogenic and can also consume dissolved oxygen and destroy aquatic life. In nature, dyes could undergo various types of reactions whose products could be more toxic and dangerous for living beings [2]. Therefore, it is important to look for efficient methods and materials for their removal. Many methods have been suggested for wastewater treatment and dyes removal, like adsorption [3, 4], biodegradation [5, 6], oxidation [7, 8], or photocatalytic degradation [7, 9–11]. Adsorption belongs to the simplest, noncomplicated, and low-cost method for removing various types of pollution, including dyes. Various types of adsorbents such as carbon-based materials [2, 12–16], chitosan [17], layered double hydroxides [3, 18, 19], cotton fibers [20], montmorillonite [21, 22], metal oxides, and metal oxide composites [23–25] have been studied for the adsorption of various dyes. Other materials that are often used to remove dyes include doped conducting polymers, like polyaniline doped by boron nitride [26], chitosan-grafted-polyaniline doped with Co_3O_4 [27], and polyaniline/Co_3O_4 nanocube composite [28], or polyaniline/$SrTiO_3$ nanocubes [29], and those composites were successfully applied in adsorption or photocatalytic degradation methyl orange and MB dyes [26–29]. These materials are becoming more popular as they offer a wide range of applications such as sensors, adsorbents, photocatalysis, and batteries [26–29]. GO and its composites belong to the aforementioned popular adsorbents [30, 31]. GO belongs to the carbonaceous materials with an ideal two-dimensional structure with carbon atoms assembled to the honeycomb structure. The presence of various types of oxygen-containing surface functional groups (carboxyl, hydroxyl, epoxy, and carbonyl) belongs among the greatest GO benefits. These surface

groups facilitate and contribute to the adsorption process via π-π stacking, hydrogen bonding, and electrostatic forces, such as van der Waals forces. They act as a weak acid cation exchange material, allow various GO modifications [32–36], and also complexation with positively charged molecules (dyes, pesticides, metal ions, etc.) [13, 14]. The information such as the GO surface hydroxyl group number and their effect on the adsorption process is limited in the scientific papers. GO-based materials with different degrees of oxidation were successfully applied in removing MB dyes with maximum adsorption capacity from 48.8 to 598.8 mg/g [37]. GO prepared by Hummer's method or GO/calcium alginate was used in MB adsorption with a maximum adsorption capacity of 476.2 mg/g and 181.8 mg/g, respectively [38, 39]. According to Chen et al. [37] and Ramesha et al. [13], reduced GO can also be involved in removing the dye, with a relatively low adsorption capacity of 91 and 17.3 mg/g, respectively. MB (Figure 1) belongs to the widely used dying agents for coloring silks, cotton, paper, temporary hair color, wools, etc. [12, 16]. It is also used in medicine, analytical redox indicator, and aquaculture [2]. MB can have some negative effects on human health, including headache, confusion, high blood pressure, and vomiting [40, 41].

In this paper, we prepared monolayer GO by a simple ultrasound exfoliation process of natural graphite with subsequent oxidation, and we compared the adsorption ability of GO at various pHs for MB removal from an aqueous solution. In order to establish the GO removal capacity, different models of isotherms (Langmuir, Langmuir-Freundlich, Temkin, and Freundlich) were fitted to the experimental data. Besides, the MB adsorption kinetics were studied, and mathematical models for the pseudo-first order and pseudo-second order were applied for measured data. The Langmuir and Langmuir-Freundlich isotherms were used to obtain the maximum adsorption capacity, whereas the Temkin model was used to evaluate some indirect interaction of MB with GO. Raman spectroscopy, transmission electron microscopy (TEM), AFM, and zeta-potential were used for GO characterization, and the data combination from these methods was used to identify and characterize the mutual interactions of MB with GO structure. The GO surface functional groups (carboxylic and hydroxyl) were determined with simple and verified acid-base titration, and the effect of GO surface functional groups on MB adsorption was discussed. The suitability of zeta-potential measurement and acid-base titration method was discussed. The FTIR and XRD were used for GO characterization and analysis of the adsorbent before and after dye adsorption and for discussion of possible adsorption mechanisms. Based on FTIR and XRD data, specific interactions of surface groups with MB were shown and confirmed.

2. Experimental

2.1. Chemicals. All purchased chemicals were analytical reagent grade. MB (≥95%; calc. to the dried substance) was purchased from Sigma-Aldrich (Germany). The chemical reagents for preparation of Britton-Robinson buffer (BRB), i.e., CH_3COOH, H_3BO_3, NaOH, and H_3PO_4 were purchased from Lach-Ner Ltd. The BRB solution was prepared according to the standard procedure published elsewhere [42]. Briefly, two solutions A and B were prepared. Solution A consists of a mixture of H_3BO_3, H_3PO_4, and CH_3COOH with the concentration of each compound at 0.04 mol/L. Next, solution B was prepared by dissolving solid NaOH to obtain a solution with a concentration of 0.02 mol/L. By mixing solutions A and B, the solutions with the required pH (3.0, 7.0, and 11.0) were prepared. The stock solution of cationic MB dye (0.5 g/L) was prepared in BRB (pH = 3.0, 7.0 and 11.0). KBr (FTIR grade, ≥99% trace metal basis) was used for FTIR measurements and was purchased from Sigma-Aldrich (Germany). Deionized water prepared by GORO Pharmpur reverse osmosis system (Goro, Czech Republic) was used for all the experiments. The chemical reagents for the synthesis of graphene oxide (GO), i.e., 96% H_2SO_4, 85% H_3PO_4, $KMnO_4$, and H_2O_2, were obtained from commercial sources Penta, Ltd. and Lach-Ner, Ltd. (Czech Republic). The natural graphite was purchased from Koh-i-noor Grafite, Ltd. (Czech Republic).

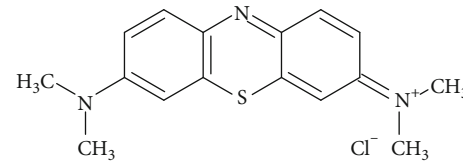

Figure 1: Methylene blue structure (CAS 61-73-4).

2.2. Preparation of Sample

2.2.1. Preparation of Graphene. Graphene sheets were prepared by exfoliation of natural graphite (1 g) in a bath ultrasound reactor UIP 2000hd (2 kHz, max. 2000 W, Hielscher Ultrasonics GmbH, Germany) under a high pressure of 5 bar in ethylene glycol (100 mL) [43]. The product was purified by dialysis with Spectra/Por 3 dialysis membrane in demineralized water to stable conductivity and constant pH.

2.2.2. Preparation of Graphene Oxide. The dried exfoliated graphite (1 g) was mixed with H_2SO_4 (60 mL) and H_3PO_4 (10 mL) in a round-bottom flask. $KMnO_4$ (3 g) was carefully added last. The reaction mixture was slowly heated to 40°C for 48 h. The additional $KMnO_4$ (1.5 g) was added in smaller doses and stirred for 3 days at the same temperature. Thereafter, the mixture was left to cool down to laboratory temperature and slowly added to the ice mixture with H_2O_2 (200 mL) [44]. The resulting product was purified by dialysis with Spectra/Por 3 dialysis membrane in demineralized water to constant pH and stable conductivity.

2.3. Characterization of Samples. The FTIR spectra were recorded on a diffuse reflectance spectrophotometer Nicolet 6700 IR (Thermo Scientific, USA) in transmittance mode in the 4000–400 cm^{-1} wavenumber range at 100 scans per spectrum with 4 cm^{-1} resolution. Software OMNIC 7.3 was used for raw data processing. The GO sample for FTIR was firstly lyophilized (24 h) and subsequently grounded with KBr in a ratio from 1 : 100 to 1 : 400 in an agate mortar

and then in a ball mill (5 min). A hydraulic press (80 kN, 5 min) was used to prepare KBr pellets of 13 mm in diameter.

Raman spectra were collected using a DXR Raman microscope (Thermo Scientific, USA) the following way: 256 two-second scans were acquired with a 532 nm laser (0.5 mW), 25 μm slit under a 10× objective Olympus microscope in full range with distinction of 2 cm^{-1}. Crystal phase analysis was performed using Bruker D2 (Germany) with the LYNXEYE 1-dimensional detector (CuKα radiation, 30 kV, 10 mA). The primary divergence slit module width of 0.6 mm, Soler Module 2.5, Airscatter screen module of 2 mm, and Ni Kbeta-filter of 0.5 mm were used in the range of 5-90°, step of 0.00805°, and time per step of 1.0 s. The XRD sample patterns after interaction with MB were processed by the following procedure. First, the GO suspension (0.1 mL) was mixed with MB solution (2.1 mL, 0.2 g/L) in 4 mL vials and were shaken for 4 h. Further, the samples were centrifuged (30 min, 10 000 RPM), washed four times with deionized water, and followed by centrifugation (shorter time). Finally, the samples were transferred to a silicon wafer, dried and measured.

Morphology of the samples deposited on microscopic copper grids covered by a transparent amorphous lacey carbon film was investigated using HRTEM FEI Talos F200X (Japan) at 120 kV. The obtained micrographs and SAED patterns (Selected area electron diffraction) were processed and evaluated by the TIA (TEM Imaging & Analysis software, FEI Company). AFM measurements were performed using Bruker Dimension Microscope (Germany) in ScanAsyst-air contact mode to determine lateral size and height profile of GO sheets. An aqueous suspension was pipetted onto mica support prior the measurement.

2.4. Titration of GO Sample. According to our procedure published in our previous work [44], acid-base titration was used to determine the number of surface functional groups, i.e., carboxylic and hydroxyl. Titration of GO sample was realized by automatic titrator 794 Basic Titrino (Metrohm, Switzerland) with potentiometric endpoint determination. GO water suspension containing 4 mg of solid in the initial volume (4 mL) was titrated with sodium hydroxide solution (0.1 mol/L) under continuous stirring and a nitrogen atmosphere. Equivalence points were evaluated from titration curves transformed in the 1st derivation curves.

2.5. Sorption Experiments. Free MB dye in an aqueous solution was evaluated and measured by the double-beam UV/VIS spectrophotometer Cintra 2020 (GBC Scientific Equipment, Australia) controlled by Cintral software vs. 2.6. All adsorption experiments were realized in the Eppendorf vials (2 mL) at 25 ± 1°C. Briefly, 100 μL of GO sample (c_{GO} = 23.5 mg/mL) and the calculated volume of MB stock solution in BRB buffer (MB concentration range 0.05–0.475 g/L) were pipetted into the vials, and vials were filled with BRB to a total volume 2 mL. To reach equilibrium, the Eppendorf vials were shaken for 3 hours (at 25 ± 1°C) and subsequently centrifuged for 30 min at 14 000 RPM. Immediately, the absorbance of free MB dye was measured by UV/VIS spectroscopy at 658 nm. The concentration of free MB dye was calculated from the measured absorbance and previously obtained calibration curves. The amount of MB dye adsorbed by GO samples at equilibrium q_E (mg/g) was calculated by

$$q_E = \frac{(c_0 - c_E)\bullet V}{m}. \quad (1)$$

The c_0 and c_E (mg/L) are the initial and equilibrium dye concentration, V (L) is the volume of solution, and m (g) is the mass of the sample in the solution.

2.6. Kinetic Study Experiment. The batch adsorption experiments in a beaker (50 mL) were used to study the adsorption kinetics. MB stock solutions in BRB (0.5 g/L, 32 mL), BRB (6 mL), and GO suspension (2 mL) were pipetted into the beaker. The initial MB concentration for the kinetic study was 400 mg/L. The beaker was placed on the magnetic stirrer. At selected times, aliquots were taken into the Eppendorf vials (2 mL). The Eppendorf vials were centrifuged for 30 min at 14 000 RPM and immediately the absorbance of free MB dye was measured by UV/VIS spectroscopy at 658 nm. The previously obtained calibration curves were used to calculate the concentration of free MB dye in the solution.

2.7. Zeta Potential Measurements. Zeta potential of prepared particles was monitored by electrophoretic light scattering (ELS) measurement performed on Lizesizer™ 500 (Anton Paar, Austria) coupled to a Metrohm automatic titrator with an 867 pH module and an 846 dosing interface controlled by the software Kalliope™. The temperature was 25°C, the initial pH was 11, and the final pH was 2, with a step of 0.5 modified with 0.5 M of HCl or NaOH with stabilization time of 5 min per step. The Smoluchowski approximation method was used.

3. Results and Discussion

3.1. Sample Characterization. The Raman spectrum (Figure 2(a)) shows typical GO bands G (~1591 cm^{-1}) and G′ bands (~2700 cm^{-1}) for E_{2g} vibrational modes, which are associated with in-plane vibration of sp^2 carbon framework. The spectrum also contains D band (~1356 cm^{-1}) describing the deformations and breathing of aromatic rings of carbon lattice [45–47]. The presence of D bands proves the presence of defects connected with oxygen-containing groups such as hydroxyl, carbonyl, carboxyl, and epoxy [48]. The distance between defects in GO structure and the number of GO layers were evaluated from I_D/I_G ratio, and for GO, it is standardly about 1 (532 nm laser excitation). According to I_D/I_G ratio, the distance between the defects varies from 1 to 3 nm [49]. The I_{2D}/I_G ratio is 0.25 (I_D/I_G = 0.94), and it generally corresponds to the multilayer GO structure (more than 5 layers) [50]. The lower I_D intensity suggests a low number of defects in the GO structure, whereas the higher I_G intensity supports the unbroken sp^2

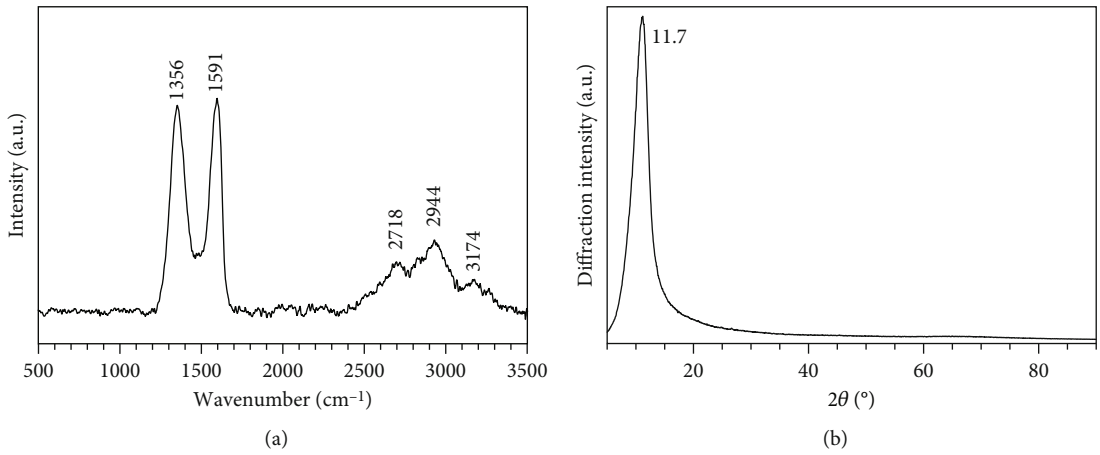

Figure 2: Raman (a) and XRD pattern (b) of prepared GO sample.

carbon framework. The G bands at 1591 cm^{-1} indicate significant disorders in GO structure due to the rough oxidation process [51]. The G and 2D bands usually located at 1581 and 2679 cm^{-1} correspond to the single graphene sheets, whereas for multilayer GO sheets, the G and 2D bands shift to higher wavenumbers (1591 and 2718 cm^{-1}). The 2D band at 2718 cm^{-1} serves as an indicator of graphene layer number [33, 52]. The S3 band at ~2944 cm^{-1} corresponds to the second-order peak derived from the combination of the D-G peak [52, 53]. The 2G band (~3174 cm^{-1}) can be attributed to the overtone of the G band [53].

XRD patterns of prepared graphene oxide (GO) are shown in Figure 2(b). A broad and very strong peak localized at 11.7° is characteristic for interplanar d_{002} spacing in GO and confirmed successful synthesis of GO sheets. The d-spacing parameter 0.79 nm indicates the presence of oxygen functionality in the interlayer spacing of the graphite skeleton [54, 55]. Typically, the interlayer distance between GO sheets ranges from 0.5 to 0.9 nm and depends on the amount and the type of intercalated groups (hydroxyl, carboxyl, carbonyl, epoxy, and H_2O molecules) [55].

HRTEM image of the prepared GO shows monolayered sheets (Figure 3(a)). In Figure 3(b), the fast Fourier transform (FFT) is shown where the points in the GO hexagonal honeycomb structure are present; i.e., it confirms that the plate is a monolayer. Figure 3(c) shows the TEM image with SEAD analysis of GO (inlet) which revealed a spot pattern, which proves single-layered GO. From the TEM image (Figure 3(c)), the presence of the monolayer is not clearly visible; therefore, the data from the AFM are present. GO AFM image shows large differences in the lateral size of GO sheets with a height profile of 1 nm in all measured cases (Figure 3(d)).

3.2. Evaluation of Surface Hydroxyl Groups. The potentiometric titration was used to evaluate surface functional groups. The measured titration curve with the 1st derivation is shown in Figure 4(a). Two equivalence points (EP1 and EP2) were present on the titration curve. According to our previous research, the EP1 corresponds to the NaOH consumed to neutralize the carboxylic groups type (q_1). In contrast, the difference between (EP2–EP1) and the NaOH consumed for the neutralization of hydroxyl type groups (q_2) [44]. The determined number of carboxylic group type (q_1) was 1.10 ± 0.04 mmol/g, and that of hydroxyl group type (q_2) was 0.96 ± 0.02 mmol/g, respectively. A slightly higher number of carboxylic functional groups were observed in comparison with the hydroxyl groups.

The measured titration curve was transformed into the curve corresponding to the total concentration of protons consumed in the titration process (TOTH, see Figure 4(b)) and can be calculated by [14, 56]

$$\mathrm{TOTH} = \frac{-(V_{\mathrm{NaOH}} - V_{\mathrm{EP1}}) \bullet c_{\mathrm{NaOH}}}{m_{\mathrm{GO}}}. \quad (2)$$

In Equation (2), c_{NaOH} and V_{NaOH} represent the analytical concentration of NaOH and the volume of NaOH added at different titration points, respectively. V_{EP1} corresponds to the volume of the first equivalent point, and m_{GO} is the weight of GO used in the titration.

The amphoteric behavior of GO surface groups provides the ability of the GO material to become positively or negatively charged depending on solution pH. The hydroxyl and carboxyl groups exhibit amphoteric behavior. The TOTH curve in Figure 4(b) shows the ability to release or associate protons per solid weight into or from the solution. The positive TOTH values represent proton association and can be described by Equation (3). In contrast, negative values represent the opposite process (Equation (4)). The GO surface becomes positively charged at low pH values due to the proton association (TOTH positive values). In contrast, the GO surface becomes negatively charged at high pH values due to the proton release (TOTH negative values) [57, 58].

$$\begin{aligned} \mathrm{GO-COOH} + \mathrm{H^+} &\leftrightarrows \mathrm{GO-COOH_2^+} \\ \mathrm{GO-OH} + \mathrm{H^+} &\leftrightarrows \mathrm{GO-OH_2^+} \end{aligned} \quad (3)$$

$$\begin{aligned} \mathrm{GO-COOH} &\leftrightarrows \mathrm{GO-COO^-} + \mathrm{H^+} \\ \mathrm{GO-OH} &\leftrightarrows \mathrm{GO-OH^-} + \mathrm{H^+} \end{aligned} \quad (4)$$

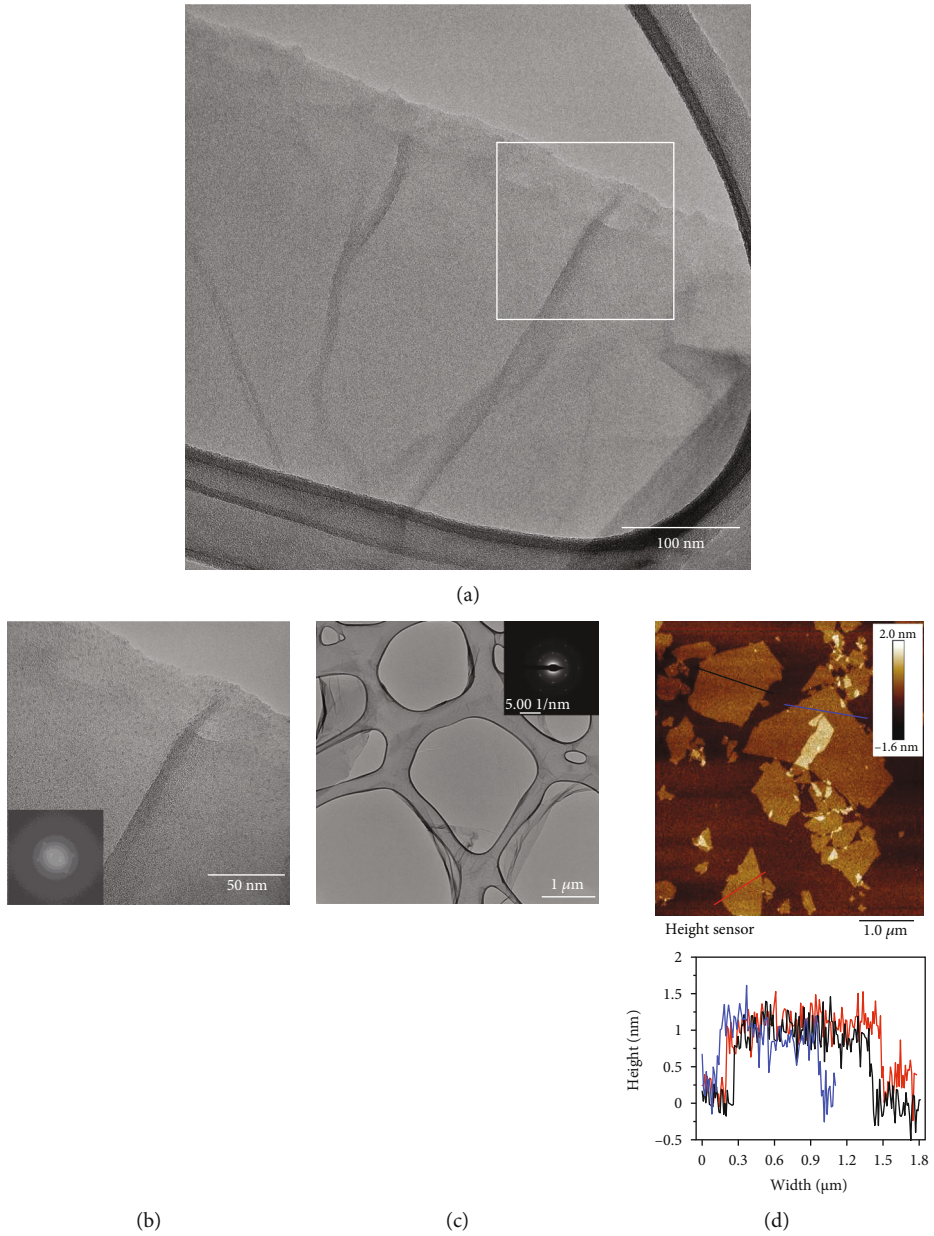

Figure 3: HRTEM image (a), FFT analysis (b), TEM image with SAED patterns (c), and AFM image with height profile (d) of GO sample.

The TOTH curve (Figure 4(b)) shows that the GO surface was positively charged below pH < 4.3, and at pH > 4.3, the GO surface was negatively charged. The TOTH curve analysis provided that the PZC corresponds to pH(PZC) = 4.3, as demonstrated [14, 56, 59].

The high degree stability of GO nanosheets was confirmed by zeta potential measurements ($\zeta = -36.7$ mV). Standardly, the nanosheets with high degrees of stability have zeta potential values greater than ±30 mV [60]. Figure 5 represents the GO zeta potential change with pH and the values are negative at all pH values studied. The data in Figure 5 suggest that the GO oxygen species are deprotonated in the whole pH range studied and the data agree with other GOs and carbon-based materials [37, 61–63]. The negative zeta potential values in acid pH showed that GO forms stable colloids due to the ionized oxygen functional groups (-COOH) electrostatic repulsion [37, 62], which helps the adsorption of positively charged MB dye. The discrepancies in pH(PZC) evaluated from TOTH curves and zeta potential measurement can be ascribed to the (a) differences in the evaluation methods used and (b) GO ageing process. The GO ageing is followed by a spontaneous chemical reaction, especially in epoxy groups deprivation and hydroxyl group enrichment [64]. Besides, the GO degradation pathway leads to humic acid-like structures and mainly occurs in the water environment [65, 66].

The isoelectric point values (IEP) represent external surface charges of nanosheets in solution, at which the zeta potential of the surface or molecule is equal to zero. The IEP value indicates the pH at which the GO nanosheets do not move in an electric field [67]. Conversely, pH(PZC) is connected to GO nanosheets' total net surface charge

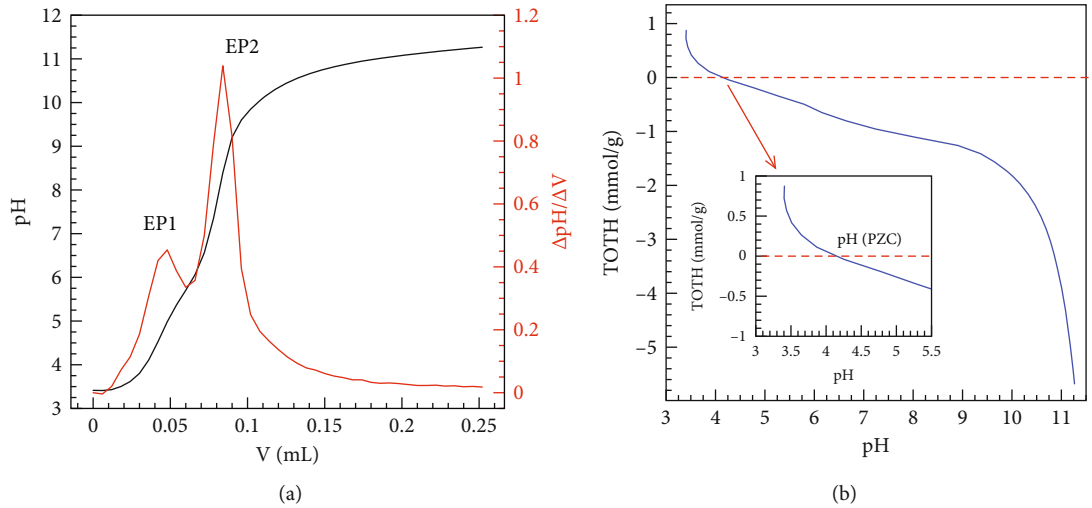

(a) (b)

Figure 4: (a) Titration curve with the 1st derivative curve of the prepared GO sample with two distinct equivalent points (EP1 and EP2). (b) Curve corresponding to the total concentration of protons consumed in the titration process (TOTH). The inset plot present pH corresponds to the point of zero charge (PZC).

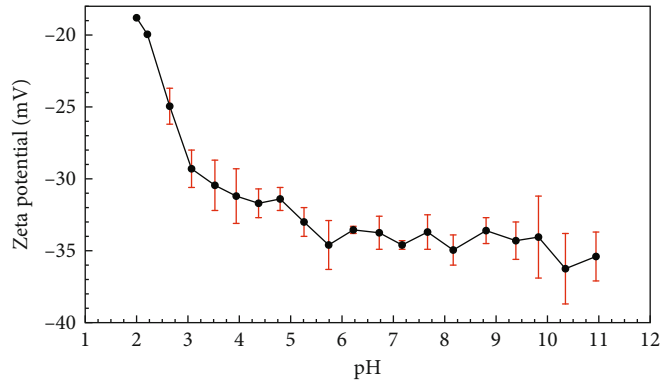

Figure 5: GO zeta potential change with pH.

distributions (internal and external). The pH(PZC) values are defined as the negative logarithm of the activity of the potential determining ions at which the net surface charge distribution is equal ($\sigma_{OH_2^+} = \sigma_{OH^-}$), as well as the surface concentrations ($[MO^-] = [MOH_2^+]$) [68–70]. The pH(IEP) and pH(PZC) values are commonly identical if no other reaction or adsorption process occurs [69]. The discrepancies in IEP and pH(PZC) indicate some specific absorption of the bulk electrolyte. The shift to lower or higher IEP values would be caused mainly by some specific adsorption of cations or anions from the background electrolyte used in zeta potential measurement [71, 72]. On the other hand, the acid-base titration is based on the transfer of OH^- and H_3O^+ ions between the GO ionizable surface groups, which is the primary process involved in acid-base titration. In contrast, zeta potential (electrophoretic mobility) corresponds to the external surface charge potential. According to Corapcioglu and Huang [73], high pH(PZC) values obtained by acid-base titration are characteristic of reduced surfaces. Conversely, the low pH(PZC) values obtained by zeta potential are typical of oxidized surfaces. In addition, Corapcioglu and Huang [73] mentioned that zeta potential measurements provide false information and acid-base titration provides better quantitative information about the surface acidity of carbon-based materials. The differences in pH(PZC) and IEP indicate higher heterogeneity of carbon-based materials and can be connected with the GO oxidation process and the degree of oxidation [67, 74].

According to Menéndez et al. [67], the relatively low value of pH(PZC) showed the high acidity of GO material and, thus, an increased number of oxygen-containing surface groups with an acidic character. Acid-base titration as well as the zeta potential methods belong to the powerful techniques for GO surface characterization.

3.3. Adsorption Isotherm Data. The adsorption isotherms describe the relationship between the adsorbent and adsorbate in the equilibrium state. The relationship between the solution dye concentration and equilibrium state has been described by the most widely used Langmuir, Freundlich, Langmuir-Freundlich, and Temkin isotherms [4, 75, 76]. The experimental data for MB adsorption in an aqueous

solution (25 ± 1°C) were evaluated using all these four types of isotherms. In Equations (5), (6), (7), and (8), c_E is the equilibrium dye concentration (mg/L), q_E is the equilibrium amount of cationic dye adsorbed per unit weight of adsorbent (mg/g), q_M is the maximum adsorption capacity (mg/g), K_L is the Langmuir adsorption constant (L/g), K_F is the Freundlich isotherm constant (L/g), n_F is the adsorption intensity, K_{LF} the equilibrium constant for heterogeneous solid (L/g), and n_{LF} is the heterogeneity parameter [77]. In the Temkin isotherm model (Equation (8)), A_T is Temkin parameter related to the equilibrium binding constant (L/g); B_T is the Temkin constant related to the adsorption heat (J/mol), and it is defined by the expression $B_T = RT/b_T$, where R is the universal gas constant (8.314 J/K mol), T is the thermodynamic temperature (K), and b_T is the Temkin constant [15, 76, 78].

Monolayer adsorption on a homogeneous surface can be described by the Langmuir (L) adsorption isotherm. The Langmuir isotherm assumes the surface with a finite number of definite localized places which are identical and equivalent [13, 79]. The Langmuir adsorption isotherm in non-linear form can be expressed by

$$q_E = q_M \bullet \frac{K_L \bullet c_E}{1 + K_L \bullet c_E}. \quad (5)$$

The Freundlich (F) adsorption isotherm is frequently used to describe the non-ideal and reversible adsorption at heterogeneous surfaces and to describe the adsorption process of organic compounds on carbon-based materials or molecular sieves [79, 80]. The formation of a monolayer is not limiting for this isotherm. The Freundlich isotherm can be expressed in non-linear form by

$$q_E = K_F \bullet c_E^{1/n_F}. \quad (6)$$

The Langmuir-Freundlich (LF) isotherm is a useful and flexible mathematical model, combining the advantages and behaviour of Freundlich and Langmuir isotherm [81]. The main advantage of LF isotherm is that, at low adsorbate concentration, it reduces to Freundlich isotherm. In contrast, at high adsorbate concentrations, it behaves as the Langmuir isotherm with monolayer adsorption capacity [79, 82]. The Langmuir-Freundlich isotherm can be expressed in a nonlinear form by

$$q_E = q_M \bullet \frac{K_{LF} \bullet {c_E}^{1/n_{LF}}}{1 + K_{LF} \bullet {c_E}^{1/n_{LF}}}. \quad (7)$$

In addition, for the evaluation of some indirect GO-MB interactions, the Temkin isotherm was used. This model suggested that the adsorption heat of all the molecules in the layer linearly decreases with coverage [78]. The Temkin isotherm in a nonlinear form can be expressed by

$$q_E = B_T \bullet \ln\left(A_T \bullet c_E\right). \quad (8)$$

MB sorption experiments were performed in acidic, neutral, and basic pH values (3.0; 7.0; 11.0). The pH effect on the MB sorption process and adsorption isotherm data are shown in Figure 6, and isotherm parameters are presented in Table 1.

In comparison with the other experiments on GO carried out by Li et al. [12] (2 times) and Ramesha et al. [13] (30 times) at pH = 3.0 and pH = 7.0, our prepared GO sample has shown higher MB sorption capacity. In contrast, at pH = 11.0, the q_M is 10 times and 140 times higher, respectively. The higher sorption capacity could probably be ascribed to the different GO synthesis procedures and the number of surface functional groups. However, GO oxidation degree strongly affects adsorption capacity to MB dye [37, 83], heavy metals (Co^{2+}) [84], or metalloid (AsO_3^{3-}) [85]. According to Yan et al. [37], the GO samples in low oxidation degree exhibit 10 times lower q_M values for MB than highly oxidized samples. Table 2 presents an adsorption capacity comparison between GO, other adsorbents, and GO/composite materials towards MB dye. The table shows the experimental conditions, maximum adsorption capacity, and mathematical model used for data fitting.

The data summarized in Table 2 show significant differences in q_M values and comparison of laboratory conditions for various GOs, active carbons, carbon nanotubes, and GO/composites from the literature. Nevertheless, our GO sample under various experimental conditions showed the highest adsorption capacity towards MB dye. The GO/composite materials did not show such high q_M values as may be expected. However, the lower absorption capacity of composites does not mean that they are inefficient materials if these composites show, e.g., photocatalytic activity, as demonstrated by Shahabuddin et al. [26, 27, 29]. The MB removal efficiency and lower q_M should probably be connected with another synthesis procedure (Hummer's, Brodie's), the number of surface hydroxyl groups, pH(PZC), defects in GO honeycomb structure, and GO oxidation degree [37, 48, 56, 91]. Similar q_M values were found for GO by Chia et al. [38]; compared to other GO materials [12, 13, 39] and GO/composites [39, 86, 87], our GO material showed at least two times higher, however, even fifty times higher q_M values. Comparable q_M values can be found for the various activated carbons [12, 16, 89] and GO [37, 38] that exhibit a relatively large surface area as well as the activation/synthesis procedure, which may play a crucial role in MB removal.

The sorption process is describable at different pH values by various mathematical models. It shows the variability of the GO behavior and its ability to eliminate MB dye from aqueous solutions at different pH values. The calculated parameters (Table 1) have shown differences in MB sorption depending on solution pH. In acidic (pH = 3.0) and basic (pH = 11.0) environment, the sorption process can be described by the Langmuir-Freundlich mathematical model ($R^2 = 0.9994$; $R^2 = 0.9842$) with maximum adsorption capacity of 440.5 mg/g (pH = 3.0) and 803.7 mg/g (pH = 11.0), respectively. Conversely, in neutral pH (pH = 7.0), the behavior can be described by Langmuir mathematical model ($R^2 = 0.9900$) with a maximum adsorption capacity of 445.9 mg/g.

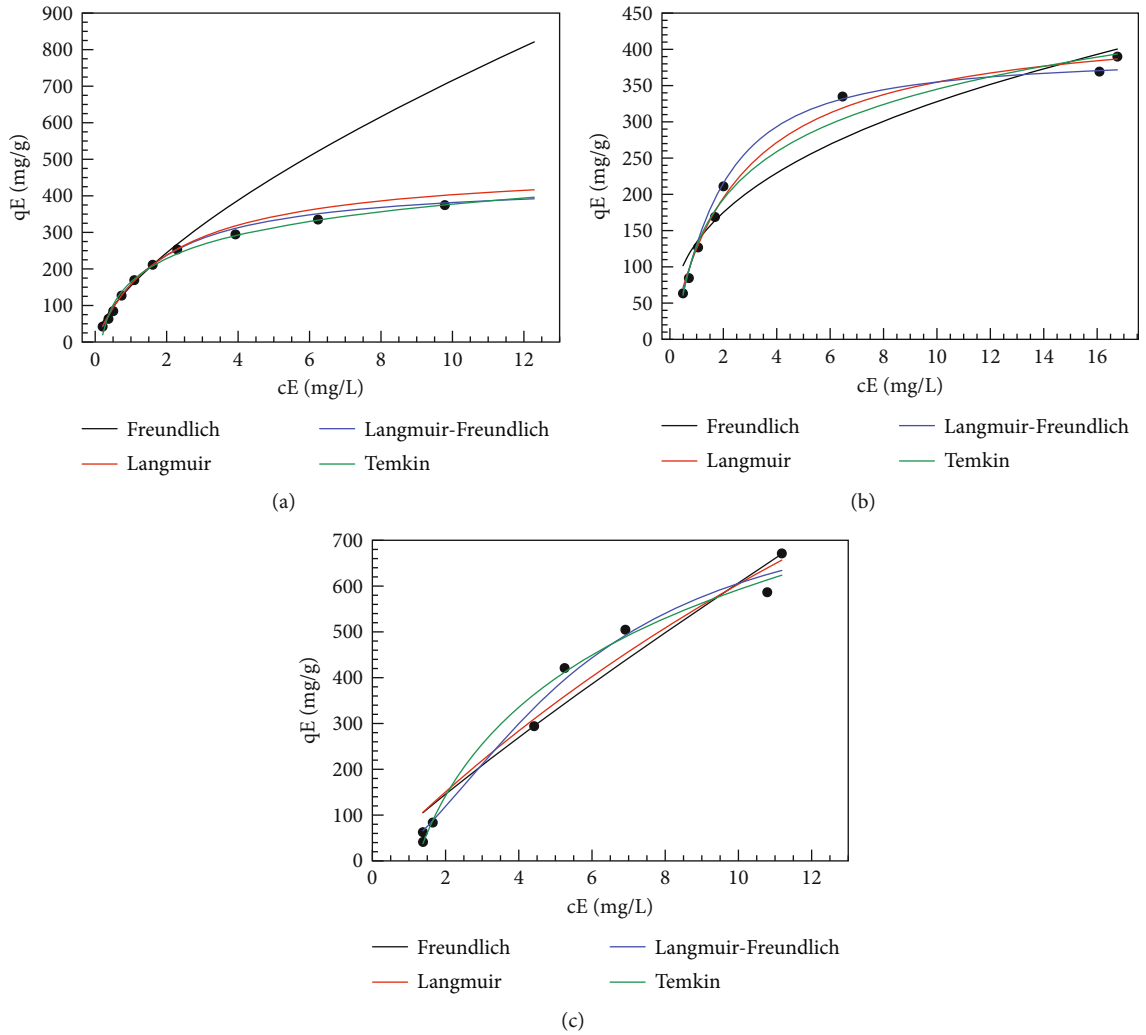

Figure 6: Fits of the Freundlich, Langmuir, Langmuir-Freundlich, and Temkin isotherms for the adsorption of MB on GO sample at pH = 3.0 (a), pH = 7.0 (b) and pH = 11.0 (c). 2.35 mg of GO; i.e., 100 μL of GO suspension, MB initial concentration range: 0.05–0.475 g/L at 298 K.

Table 1: Freundlich, Langmuir, Langmuir-Freundlich, and Temkin model constants and correlation coefficients for the adsorption of MB by GO sample.

pH	Freundlich			Langmuir			Langmuir-Freundlich				Temkin			
	K_F (L/mg)	n_F	R^2	K_L (L/mg)	q_M (mg/g)	R^2	K_{LF} (L/mg)	q_M (mg/g)	n_{LF}	R^2	A_T (L/mg)	B_T	R^2	b_T (J/mol)
3.0	0.154	1.49	0.9770	0.476	487.7	0.9990	0.560	440.5	0.940	0.9994	5.95	92.3	0.9918	26.9
7.0	0.134	2.58	0.9211	0.389	445.9	0.9900	0.500[a]	391.1	0.773	0.9858	3.91	94.1	0.9809	26.3
11.0	0.079	1.13	0.9415	0.033	2441.1	0.9530	0.050[a]	803.7	0.560	0.9842	0.83	280.1	0.9765	8.85

[a]Fixed parameters.

The Langmuir, Langmuir-Freundlich, and Temkin models appear to be the most suitable for the description of the MB sorption by GO under our conditions. The mathematical models (L and LF) suggested the creation of MB monolayer with GO active sites, which are identical and homogeneously distributed on the GO surface [16, 87]. Conversely, the Temkin mathematical model was used to evaluate the indirect MB-GO interaction. According to R^2 values, the Temkin model can be evidently also used to describe MB on GO. The data obtained by a nonlinear fitting (Temkin model) suggested the presence of various indirect MB interactions with GO surface. Those indirect interactions probably come from the MB interactions with functional groups and GO carbon honeycomb structure (see Figure 7). The Temkin equilibrium binding constant A_T decreases with increasing pH to the lowest value of 0.83 L/mg at pH 11.0.

Table 2: Comparison of GO adsorption capacity towards MB with other values from the literature.

Adsorbent	q_M (mg/g)	Mathematical model*	pH	Temperature (K)	Refs.
GO	440.5	LF	3.0	298	This work
GO	445.9	L	7.0	298	This work
GO	803.7	LF	11.0	298	This work
GO	476.2	L	NA	293	[38]
GO	144.9	L	5.4	298	[39]
GO	243.9	L	6.0	298	[12]
GO (various oxidation degrees)	40.6 – 570.4	L	7.0	298	[37]
Active carbon	270.3	L	6.0	298	[12]
GO/calcium alginate	181.8	L	5.4	298	[39]
GO	17.3	L	NA	NA	[13]
GO/polyaniline	6.7	L	NA	298	[86]
GO/magnetic cellulose composite	70.0	L	NA	298	[87]
Magnetic multi/wall carbon nanotube	11.86	L	7.0	298	[88]
Activated carbon	375	L	4 - 5	298	[89]
Modified expanded graphite powder	0.0077	L	7.0	293	[90]

*LF: Langmuir-Freundlich mathematical model; L: Langmuir mathematical model.

The Temkin constant b_T related to the sorption heat decreased with increasing pH to the lowest value of 8.85 J/mol at pH 11.0 (Table 1). The positive Temkin constant b_T values (for all pH) indicate that the MB adsorption onto GO is an exothermic reaction. With the increasing pH, the adsorption reaction is less exothermic.

In contrast, the Freundlich mathematical model is not suitable for the description of MB adsorption concerning R^2. According to the calculated Langmuir constant, the affinity of MB sorption decreases at higher pH values.

The higher sorption ability of the GO sample is dependent on the pH. It can be most likely explained by the deprotonation of the GO surface functional groups, which support MB interaction with negatively charged GO surface [2, 92]. According to data published elsewhere, the GO materials with rich oxygen-containing functional groups showed and played an essential role in the increased adsorption capacity to radioactive iodine [93], arsenic(III) [85], cadmium [94], and MB [48, 91]. Oxygen-containing functional groups enable the formation of covalent bonding, electrostatic attraction, and cation exchange with MB dye. The MB adsorption mechanism can be attributed to (a) electrostatic/ionic interactions of positively charged MB structure with negatively charged –OH, carboxyl, carbonyl, and epoxy groups on the basal plane and edges of GO and (b) π-π interaction and conjugation based on the electron donor-acceptor interaction with honeycomb GO structure (see Figure 7). The adsorption mechanism involves mainly the interaction of π electrons in C=C bond in MB structure with the π electrons in the GO honeycomb structure [48, 91, 95].

Maximum adsorption capacity (L and LF) supports the above-mentioned effect of surface groups. The pH value greatly affects MB sorption, as demonstrated [2, 13], but contradicts the results of Liu et al. [92]. Adsorption efficiency for MB removal (at measured pH) achieved 98.2% (pH = 3.0), 99.2% (pH = 7.0), and 99.0% (pH = 11.0) for initial MB concentration of 400 mg/L. The adsorption efficiencies are similar for carbon nanotubes (<98.8%) [88], activated carbon (90%) [16], and cellulose/GO composite (96.7%) [87], but not so high for GO/calcium alginate composite (83.7%) [39] and carbon nanotubes (≈ 75%) [12] in comparison with data published elsewhere.

A heterogeneity parameter ($n_F > 1$) shows that MB sorption is the physical process at all pH values. The value ($1/n_F$) suggested the standard MB sorption process. According to our results (data not shown), calculated values ($n_F > 1$; $1/n_F < 1$) show that the Freundlich model is suitable for the description of MB sorption onto GO sample (at measured pH values) [79], despite the correlation coefficient.

Besides that, we calculated the separation factor (R_L, Equation (9)) from Langmuir isotherm (data not shown). The R_L value was used for evaluation and confirmation, whether the sorption is unfavorable ($R_L > 1$), linear ($R_L = 1$), or favorable ($0 < R_L < 1$).

$$R_L = \frac{1}{1 + K_L \bullet c_E}. \quad (9)$$

Calculated values (0.05–0.475 g/L MB concentration range) have shown a favorable MB sorption process onto the GO sample under our experimental conditions. As shown in Figure 8, R_L value decreases with increasing initial concentration (c_0) (at measured pH values), suggesting the MB sorption is more favorable at a higher MB concentration [16]. At pH 3.0 and 7.0, the dependence R_L on c_0 has shown a similar trend. Conversely, at pH 11.0, the decline is not so steep; it is evident that the MB adsorption process also becomes more favorable at a relatively high MB concentration.

3.4. Kinetics Studies. To evaluate the effectiveness of the pH solution on the MB adsorption, the plot in Figure 9 shows the amount of MB adsorbed q_T at time t. The initial

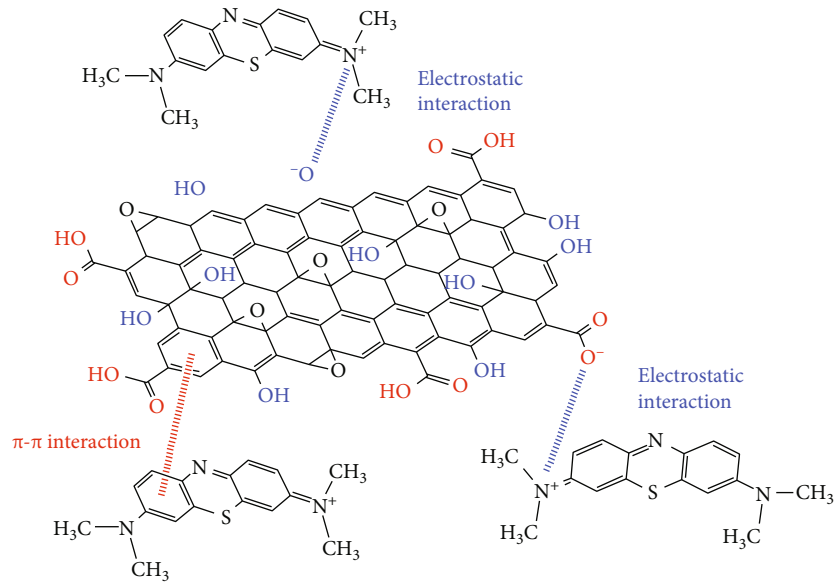

Figure 7: Potential interactions of MB dye with GO surface.

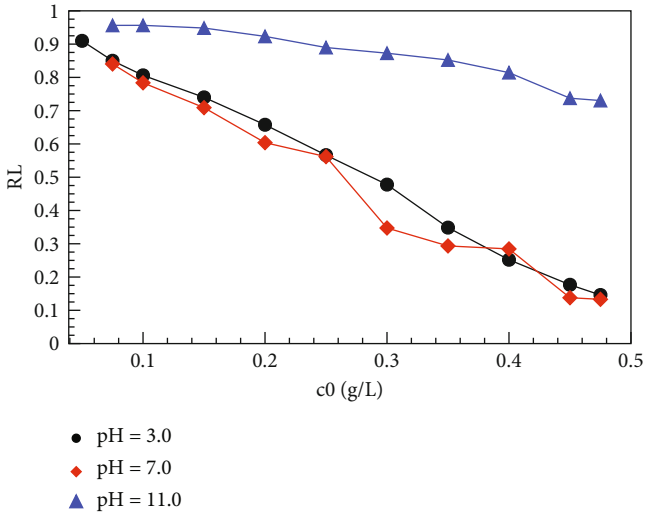

Figure 8: Separation factor value (R_L) depending on the MB initial concentration (c_0). MB initial concentration range of 0.05–0.475 g/L at 298 K.

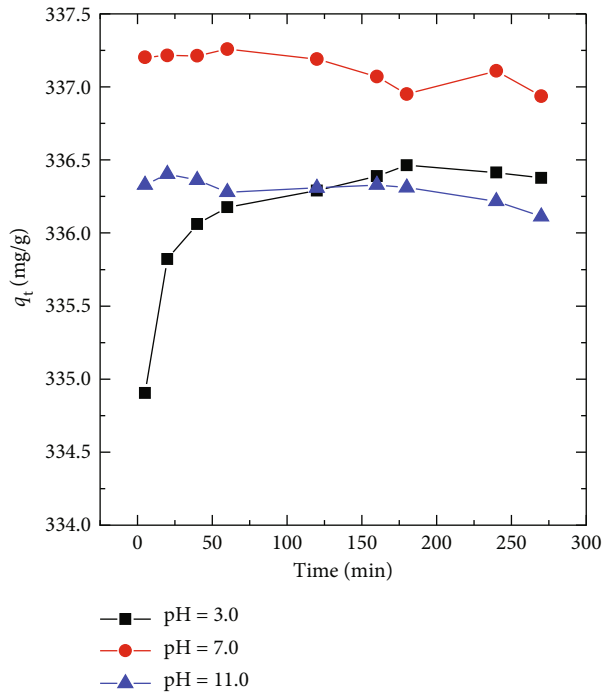

Figure 9: The adsorption kinetics of MB at pH = 3.0 (■), pH = 7.0 (●), and pH = 11.0 (▲). Initial MB concentration of 0.5 g/L and 2 mL of GO suspension, i.e., 47 mg of GO at 298 K.

adsorption stage is rapid for pH 7.0 and 11.0, which could be ascribed to partly and fully deprotonated GO surface groups. Conversely, the initial adsorption stage at pH 3.0 was relatively slow, and the maximum was achieved after 180 min. The slow initial adsorption stage at pH 3.0 (Figure 9) can be attributed to the complicated adsorption process, which could be connected to the mutual competition of MB dye and other ions, mainly with protons, in solution with positively charged GO surface groups. The π-π interactions of MB with the GO honeycomb structure are probably the primary type of MB interaction with the GO structure [2, 12]. GO sheets at lower pH values aggregated together and could play a role in the lower adsorption capacity and slow adsorption process. Negatively charged GO sheets and the electrostatic repulsion between sheets with increasing solution pH could be helpful for MB adsorption [86, 96], as is evident from our measured data.

To investigate the adsorption kinetics of MB dye on the GO, the pseudosecond-order kinetics model (10) and pseudofirst-order model (11) were tested. The

Table 3: The adsorption kinetics parameters for MB adsorption on the GO.

pH	Pseudosecond order			Pseudofirst order		
	q_E (mg/g)	k_2 (min g/mg)	R^2	q_E (mg/g)	k_1 (min^{-1})	R^2
3.0	336.4	0.080	1.0000	336.2	1.10	0.8034
7.0	336.9	0.101	1.0000	337.1	3.9×10^4	−0.1429
11.0	336.2	0.106	1.0000	336.3	1.3×10^6	−0.1667

pseudosecond-order and pseudofirst-order kinetics model in a nonlinear form can be expressed by [12, 97]

$$q_t = \frac{q_E^2 \bullet k_2 \bullet t}{q_E \bullet k_2 \bullet t + 1}, \quad (10)$$

$$q_t = q_E \bullet \left(1 - e^{-k_1 \bullet t}\right), \quad (11)$$

where q_E and q_t are the adsorption capacity (mg/g) at equilibrium and at time t (min), respectively, and k_2 (min g/mg) and k_1 (min^{-1}) are the rate adsorption constants. The parameters of pseudo-second order can be calculated from the plot of (t/q_t) vs. t (plot not shown). The results are presented in Table 3. The results showed that the pseudo-second-order model was better than the pseudo-first-order model for MB adsorption on the GO, which is in agreement with other literatures [92, 98]. Conversely, the pseudofirst order is partly suitable for the description of MB adsorption only in acidic pH, but unsuitable at neutral and basic pH, as evident from the correlation coefficient. Moreover, the rate constant of the adsorption increases with increasing pH, suggesting faster kinetic of MB adsorption at the higher pH solution.

The mutual correlation of measured and calculated parameters is complicated. Thus, we tried a correlation between the maximum adsorption capacity (q_M), a model solution pH, and the adsorption rate constant (k_2) (see Figure 10). The main effect of increasing pH is evident in the adsorption rate constant (pH = 3 vs. pH = 11), and the change in maximum adsorption capacity (pH = 3 and pH = 7 vs. pH = 11) is significant, as shown in Figure 10. Basic solution pH values mainly affect q_M values, and the increase in adsorption rate constant is insignificant. The k_2 value variates from 0.08 to 0.106 min g/min for pH = 3 and pH = 11, respectively.

3.5. Characterization of Samples before and after Sorption of MB by FTIR. The FTIR spectra of prepared GO sample are shown in Figure 11. The most intensive bands are localized in the 3800–3000 cm^{-1} region, corresponding to the stretching vibration of O—H bonds in hydroxyl from carboxyl groups and residual water intercalated in the GO sheets. The further bands were localized in the 2000–1000 cm^{-1} fingerprint region. The vibration band found at 1732 cm^{-1} is the characteristic of stretching vibration of C=O bonds in carboxylic groups [99–101]. The C=C stretching vibration (for carbon with sp^2 hybridization) in GO was localized at

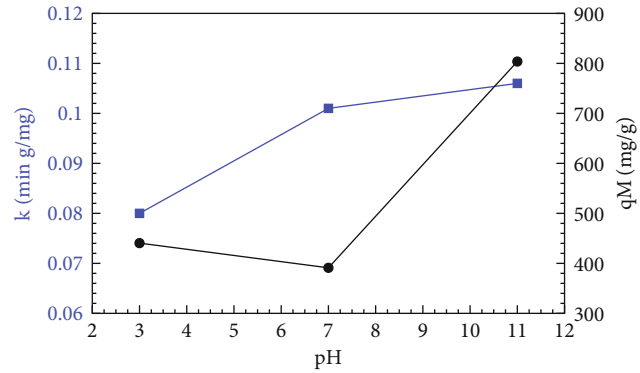

Figure 10: Mutual correlation of maximum adsorption capacity q_M vs. model solution pH (●) and adsorption rate constant k_2 vs. q_M (■) for MB removal by GO.

1625 cm^{-1} [56, 100, 101]. The bands corresponding to the bending and stretching vibration of alkoxide (C—O) and epoxides (C—O—C) functional groups were found at 1226 and 1078 cm^{-1} [99–101].

The FTIR spectra of MB dye are shown in Figure 11. The fundamental bands are localized in the 1800–600 cm^{-1} region. The stretching vibration bands corresponding to the $C_{het}=N^+(CH_3)_2$ bonds were found at 1648 cm^{-1}. The intensive stretching vibration of C=C and C=N bonds is localized at 1600 cm^{-1}. The stretching vibration of C—N and C—C bond of heterocycle was found at 1540 and 1225 cm^{-1} and the deformation vibration of C—N bond of heterocycle at 1143 cm^{-1}. The $C=S^+$ stretching vibration of MB heterocycle is seen at 1491 and 1355 cm^{-1}. The next bands localized at 1446 and 1398 cm^{-1} can be ascribed to asymmetric and symmetric deformation vibration of C—H bond in $N(CH_3)_2$. The stretching vibration of C—N in $N—CH_3$ is found at 1340 cm^{-1} and deformation and bending out-of-plane vibration of C—H at 1251, 1225, and 1189 cm^{-1}. Finally, the C—S—C bond vibration of MB heterocycle is located at 1069 cm^{-1}. All these vibrations correspond with the literature [102–104].

The FTIR spectra shown in Figure 11 correspond to the GO after sorption of MB dye. It should be mentioned that the intensity of characteristic GO bands decreased, particularly the intensity of the characteristic stretching vibration of (O—H) bonds in 3800–3000 cm^{-1} region. The vibration band at 1730 cm^{-1} corresponding to C=O bonds in carboxylic groups nearly disappeared, the band at 1625 cm^{-1} slightly shifted to 1638 cm^{-1}, and the intensity also decreased for C=C stretching vibration. The most intensive bands of MB were also found in the sample of GO after MB adsorption as 1491, 1398, 1355, and 1340 cm^{-1}. Only two vibration bands were slightly shifted at 1143 and 1069 cm^{-1} to 1149 and 1074 cm^{-1}, corresponding to deformation vibration of C—N and stretching vibration of C—S—C of heterocycle of MB (Figure 11). The attenuation of the GO bands could be ascribed to covering of GO sheets by MB and just slight shifting tends to the suggestion that most probably π-π interaction coming from aromatic rings of MB and GO is present [16, 87].

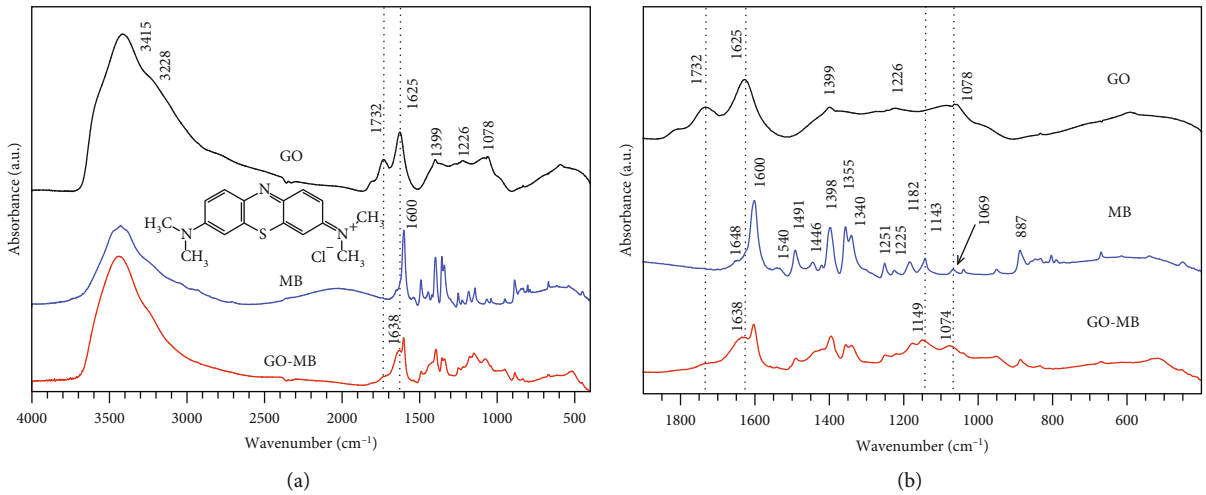

Figure 11: (a) FTIR spectra of prepared GO sample, MB cationic dye, and GO with adsorbed MB dye, details of the fingerprint region on (b).

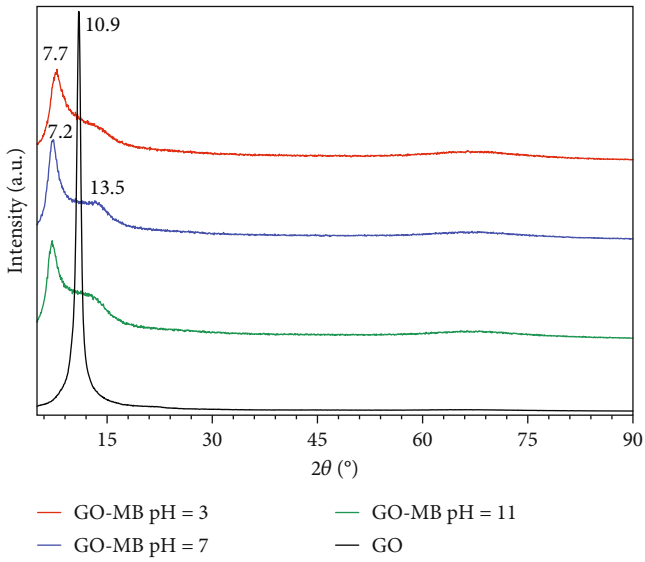

Figure 12: XRD patterns of GO before and after sorption MB at pH 3, pH 7, and pH 11.

3.6. Characterization of Samples before and after Sorption of MB by Powder XRD. The mechanism of MB adsorption was studied by Bujdák et al. [105], where orientations of MB cation were compared with experimental data. The calculated height of the MB cation is 0.77 nm. The arrangements of MB cation as intercalated dimer and monomer were determined and compared with the results obtained by Bujdák et al. [105]. The interlayer space was found to be at the range 7.2°–7.7° 2Θ corresponding to ~1.15-1.25 nm and monomeric arrangement of MB cations for all samples after sorption of MB at pH 3, 7, and 11 (Figure 12). The zones with no occupancy by MB cation were confirmed by the presence of large diffraction line at the range 10.9°–13.5° 2Θ (~0.81-0.66 nm). So, the interlayer space decreases significantly by the absence of MB cation.

4. Conclusions

Graphene oxide prepared by a simple and low-cost verified synthesis process can serve as an effective sorbent for removing dyes in effluents or other contaminated waters. We have shown a higher GO adsorption capacity for MB removal in the whole pH range compared to other works [12, 13, 37, 38, 83] and GO-based composites. Solution pH plays a crucial role in the MB removal by GO and also affects the dissociation degree of surface functional groups, i.e., hydroxyl and carboxyl. The number of surface groups was determined by acid-base titration, and IEP was evaluated by zeta potential measurement. Negatively charged oxygen-containing groups in the whole studied pH range were confirmed. According to MB kinetic adsorption studies at pH = 3.0, MB adsorption is complicated and slower due to the competition of MB with protons and positively charged functional groups on the GO surface. The increase of pH solution facilitated the MB adsorption via negatively charged GO surface and electrostatic repulsion. The purity of the prepared GO samples was proved by Raman spectroscopy and XRD; the good quality of the sheets was confirmed by TEM and AFM. The FTIR spectroscopy confirmed that the MB covering of GO sheet made the vibration spectrum of GO generally less intensive. Just slight shifting was found for C=C stretching vibration of GO and deformation vibration of C—N and stretching vibration of C—S—C of heterocycle of MB. Therefore, only electrostatic interaction, π-π interaction of aromatic rings of MB, and GO could be present. The higher sorption capacity of GO to MB dye and the other dyes belongs to the benefits of our prepared material, as we have shown in our previous paper [106]. The MB adsorption process can be described by the Langmuir-Freundlich mathematical model in acidic and alkaline pH, whereas by the Langmuir model in neutral pH. The Temkin model suggested various indirect MB interactions with the GO surface and the adsorption as an exothermic process. The applied mathematical models indicated that the MB adsorption on

the GO is a chemisorption process based on the ionic bonds and weak chemical interaction formed between MB and GO.

Data Availability

The data is stored in the repositories of the institutions listed in the manuscript or can be provided on request. For data, please contact Dr. Jakub Ederer (jakub.ederer@ujep.cz).

Additional Points

Highlights. (i) GO sheets of good quality had large lateral size. (ii) The adsorption mechanism is via π-π and electrostatic interaction. (iii) The interaction of GO with MB dye was studied by FTIR. (iv) GO sheets can be used efficiently to remove cationic dyes in the whole pH range.

Conflicts of Interest

The authors declare no conflicts of interest.

Acknowledgments

The authors acknowledge the assistance provided by the Research Infrastructure NanoEnviCz, supported by the Ministry of Education, Youth and Sports of the Czech Republic under Project No. LM2018124, and supported under the project with No. UJEP-IGA-JR-2021-44-002-2 by the Internal Grant Agency UJEP and by the Technology Agency of the Czech Republic, project TH04030285.

References

[1] S. Sheshmani, A. Ashori, and S. Hasanzadeh, "Removal of acid Orange 7 from aqueous solution using magnetic graphene/chitosan: a promising nano-adsorbent," *International Journal of Biological Macromolecules*, vol. 68, pp. 218–224, 2014.

[2] W. Zhang, C. Zhou, W. Zhou et al., "Fast and considerable adsorption of methylene blue dye onto graphene oxide," *Bulletin of Environmental Contamination and Toxicology*, vol. 87, no. 1, pp. 86–90, 2011.

[3] O. Mrózek, P. Ecorchard, P. Vomáčka et al., "Mg-Al-La LDH-$MnFe_2O_4$ hybrid material for facile removal of anionic dyes from aqueous solutions," *Applied Clay Science*, vol. 169, pp. 1–9, 2019.

[4] V. K. Konaganti, R. Kota, S. Patil, and G. Madras, "Adsorption of anionic dyes on chitosan grafted poly(alkyl methacrylate)s," *Chemical Engineering Journal*, vol. 158, no. 3, pp. 393–401, 2010.

[5] C. Palma, A. Carvajal, C. Vásquez, and E. Contreras, "Wastewater treatment for removal of recalcitrant compounds: a hybrid process for decolorization and biodegradation of dyes," *Chinese Journal of Chemical Engineering*, vol. 19, pp. 621–625, 2011.

[6] X. Xiao, T.-T. Li, X.-R. Lu et al., "A simple method for assaying anaerobic biodegradation of dyes," *Bioresource Technology*, vol. 251, pp. 204–209, 2018.

[7] O. Türgay, G. Ersöz, S. Atalay, J. Forss, and U. Welander, "The treatment of azo dyes found in textile industry wastewater by anaerobic biological method and chemical oxidation," *Separation and Purification Technology*, vol. 79, no. 1, pp. 26–33, 2011.

[8] S. Khorramfar, N. M. Mahmoodi, M. Arami, and H. Bahrami, "Oxidation of dyes from colored wastewater using activated carbon/hydrogen peroxide," *Desalination*, vol. 279, no. 1-3, pp. 183–189, 2011.

[9] J. Zhang, Z. Xiong, and X. S. Zhao, "Graphene–metal–oxide composites for the degradation of dyes under visible light irradiation," *Journal of Materials Chemistry*, vol. 21, no. 11, p. 3634, 2011.

[10] Y. Ou, J.-D. Lin, H.-M. Zou, and D.-W. Liao, "Effects of surface modification of TiO_2 with ascorbic acid on photocatalytic decolorization of an azo dye reactions and mechanisms," *Journal of Molecular Catalysis A: Chemical*, vol. 241, no. 1-2, pp. 59–64, 2005.

[11] S.-J. Zhang, H.-Q. Yu, and Q.-R. Li, "Radiolytic degradation of acid Orange 7: a mechanistic study," *Chemosphere*, vol. 61, no. 7, pp. 1003–1011, 2005.

[12] Y. Li, Q. Du, T. Liu et al., "Comparative study of methylene blue dye adsorption onto activated carbon, graphene oxide, and carbon nanotubes," *Chemical Engineering Research and Design*, vol. 91, no. 2, pp. 361–368, 2013.

[13] G. K. Ramesha, A. Vijaya Kumara, H. B. Muralidhara, and S. Sampath, "Graphene and graphene oxide as effective adsorbents toward anionic and cationic dyes," *Journal of Colloid and Interface Science*, vol. 361, no. 1, pp. 270–277, 2011.

[14] X. Yang, C. Chen, J. Li, G. Zhao, X. Ren, and X. Wang, "Graphene oxide-iron oxide and reduced graphene oxide-iron oxide hybrid materials for the removal of organic and inorganic pollutants," *RSC Advances*, vol. 2, no. 23, p. 8821, 2012.

[15] D. Robati, B. Mirza, M. Rajabi et al., "Removal of hazardous dyes-BR 12 and methyl orange using graphene oxide as an adsorbent from aqueous phase," *Chemical Engineering Journal*, vol. 284, pp. 687–697, 2016.

[16] A. M. M. Vargas, A. L. Cazetta, M. H. Kunita, T. L. Silva, and V. C. Almeida, "Adsorption of methylene blue on activated carbon produced from flamboyant pods (*Delonix regia*): study of adsorption isotherms and kinetic models," *Chemical Engineering Journal*, vol. 168, no. 2, pp. 722–730, 2011.

[17] G. G. Maghami and G. A. F. Roberts, "Studies on the adsorption of anionic dyes on chitosan," *Die Makromolekulare Chemie*, vol. 189, pp. 2239–2243, 1988.

[18] I. M. Ahmed and M. S. Gasser, "Adsorption study of anionic reactive dye from aqueous solution to Mg-Fe- CO_3 layered double hydroxide (LDH)," *Applied Surface Science*, vol. 259, pp. 650–656, 2012.

[19] R. Extremera, I. Pavlovic, M. R. Pérez, and C. Barriga, "Removal of acid orange 10 by calcined Mg/Al layered double hydroxides from water and recovery of the adsorbed dye," *Chemical Engineering Journal*, vol. 213, pp. 392–400, 2012.

[20] C. Kaewprasit, E. Hequet, N. Abidi, and J. P. Gourlot, "Application of methylene blue adsorption to cotton fiber specific surface area measurement: part I. methodology," *The Journal of Cotton Science*, vol. 2, pp. 164–173, 1998.

[21] G. Chen, J. Pan, B. Han, and H. Yan, "Adsorption of methylene blue on montmorillonite," *Journal of Dispersion Science and Technology*, vol. 20, no. 4, pp. 1179–1187, 1999.

[22] P. T. Hang and G. W. Brindley, "Methylene blue absorption by clay minerals. Determination of surface areas and cation exchange capacities (clay-organic studies XVIII)," *Clays and Clay Minerals*, vol. 18, no. 4, pp. 203–212, 1970.

[23] G. Zhang, J. Qu, H. Liu, A. T. Cooper, and R. Wu, "CuFe2O4/activated carbon composite: a novel magnetic adsorbent for the removal of acid orange II and catalytic regeneration," *Chemosphere*, vol. 68, no. 6, pp. 1058–1066, 2007.

[24] S. Recillas, J. Colón, E. Casals et al., "Chromium VI adsorption on cerium oxide nanoparticles and morphology changes during the process," *Journal of Hazardous Materials*, vol. 184, no. 1-3, pp. 425–431, 2010.

[25] K. Y. Kumar, H. B. Muralidhara, Y. A. Nayaka, J. Balasubramanyam, and H. Hanumanthappa, "Low-cost synthesis of metal oxide nanoparticles and their application in adsorption of commercial dye and heavy metal ion in aqueous solution," *Powder Technology*, vol. 246, pp. 125–136, 2013.

[26] S. Shahabuddin, R. Khanam, M. Khalid et al., "Synthesis of 2D boron nitride doped polyaniline hybrid nanocomposites for photocatalytic degradation of carcinogenic dyes from aqueous solution," *Arabian Journal of Chemistry*, vol. 11, no. 6, pp. 1000–1016, 2018.

[27] S. Shahabuddin, N. M. Sarih, F. H. Ismail, M. M. Shahid, and N. M. Huang, "Synthesis of chitosan grafted-polyaniline/Co_3O_4nanocube nanocomposites and their photocatalytic activity toward methylene blue dye degradation," *RSC Advances*, vol. 5, no. 102, pp. 83857–83867, 2015.

[28] S. Shahabuddin, N. M. Sarih, S. Mohamad, and S. N. Atika Baharin, "Synthesis and characterization of Co_3O_4nanocube-doped polyaniline nanocomposites with enhanced methyl orange adsorption from aqueous solution," *RSC Advances*, vol. 6, no. 49, pp. 43388–43400, 2016.

[29] S. Shahabuddin, N. M. Sarih, S. Mohamad, and J. J. Ching, "$SrTiO_3$ nanocube-doped polyaniline nanocomposites with enhanced photocatalytic degradation of methylene blue under visible light," *Polymers*, vol. 8, no. 2, p. 27, 2016.

[30] M. Bubeníková, P. Ecorchard, L. Szatmáry, O. Mrózek, P. Salačová, and J. Tolasz, "Sorption of Sr(II) onto nanocomposites of graphene oxide-polymeric matrix," *Journal of Radioanalytical and Nuclear Chemistry*, vol. 315, no. 2, pp. 263–272, 2018.

[31] S. H. Rashed, A. I. Abd-Elhamid, S. Y. H. Abdalkarim et al., "Preparation and characterization of layered-double hydroxides decorated on graphene oxide for dye removal from aqueous solution," *Journal of Materials Research and Technology*, vol. 17, pp. 2782–2795, 2022.

[32] R. Sitko, B. Zawisza, and E. Malicka, "Graphene as a new sorbent in analytical chemistry," *Trends in Analytical Chemistry*, vol. 51, pp. 33–43, 2013.

[33] H. Guo, T. Jiao, Q. Zhang, W. Guo, Q. Peng, and X. Yan, "Preparation of graphene oxide-based hydrogels as efficient dye adsorbents for wastewater treatment," *Nanoscale Research Letters*, vol. 10, no. 1, p. 931, 2015.

[34] S. Chen, J. Zhu, X. Wu, Q. Han, and X. Wang, "Graphene oxide–MnO_2nanocomposites for supercapacitors," *ACS Nano*, vol. 4, no. 5, pp. 2822–2830, 2010.

[35] H. Zhang, L. Lin, N. Hu et al., "Pillared decorated reduced graphene oxide film for pressure sensors with ultra-wide operation range in motion monitoring," *Carbon N. Y.*, vol. 189, pp. 430–442, 2022.

[36] M. A. A. M. Abdah, M. Mokhtar, L. T. Khoon et al., "Synthesis and electrochemical characterizations of poly(3,4-ethylenedioxythiophene/manganese oxide) coated on porous carbon nanofibers as a potential anode for lithium-ion batteries," *Energy Reports.*, vol. 7, pp. 8677–8687, 2021.

[37] H. Yan, X. Tao, Z. Yang et al., "Effects of the oxidation degree of graphene oxide on the adsorption of methylene blue," *Journal of Hazardous Materials*, vol. 268, pp. 191–198, 2014.

[38] C. H. Chia, N. F. Razali, M. S. Sajab, S. Zakaria, N. M. Huang, and H. N. Lim, "Methylene blue adsorption on graphene oxide," *Sains Malaysiana*, vol. 42, pp. 819–826, 2013.

[39] Y. Li, Q. Du, T. Liu et al., "Methylene blue adsorption on graphene oxide/calcium alginate composites," *Carbohydrate Polymers*, vol. 95, no. 1, pp. 501–507, 2013.

[40] M. Albert, M. S. Lessin, and B. F. Gilchrist, "Methylene blue: dangerous dye for neonates," *Journal of Pediatric Surgery*, vol. 38, no. 8, pp. 1244-1245, 2003.

[41] N. Wang, J. Chen, J. Wang, J. Feng, and W. Yan, "Removal of methylene blue by polyaniline/TiO_2 hydrate: adsorption kinetic, isotherm and mechanism studies," *Powder Technology*, vol. 347, pp. 93–102, 2019.

[42] H. T. S. Britton and R. A. Robinson, "CXCVIII.—universal buffer solutions and the dissociation constant of veronal," *Journal of the Chemical Society*, pp. 1456–1462, 1931.

[43] V. Štengl, "Preparation of graphene by using an intense cavitation field in a pressurized ultrasonic reactor," *Chemistry - A European Journal*, vol. 18, no. 44, pp. 14047–14054, 2012.

[44] J. Ederer, P. Janoš, P. Ecorchard et al., "Quantitative determination of acidic groups in functionalized graphene by direct titration," *Reactive and Functional Polymers*, vol. 103, pp. 44–53, 2016.

[45] R. Saito, M. Hofmann, G. Dresselhaus, A. Jorio, and M. S. Dresselhaus, "Raman spectroscopy of graphene and carbon nanotubes," *Advances in Physics*, vol. 60, no. 3, pp. 413–550, 2011.

[46] L. Peng, Z. Xu, Z. Liu et al., "An iron-based green approach to 1-h production of single-layer graphene oxide," *Nature Communications*, vol. 6, no. 1, p. 5716, 2015.

[47] V. N. Popov and P. Lambin, "Theoretical Raman intensity of the G and 2D bands of strained graphene," *Carbon*, vol. 54, pp. 86–93, 2013.

[48] L. Chen, J. Yang, X. Zeng, L. Zhang, and W. Yuan, "Adsorption of methylene blue in water by reduced graphene oxide: effect of functional groups," *Materials Express*, vol. 3, no. 4, pp. 281–290, 2013.

[49] S. Eigler, C. Dotzer, and A. Hirsch, "Visualization of defect densities in reduced graphene oxide," *Carbon*, vol. 50, no. 10, pp. 3666–3673, 2012.

[50] Y. Bleu, F. Bourquard, A. S. Loir, V. Barnier, F. Garrelie, and C. Donnet, "Raman study of the substrate influence on graphene synthesis using a solid carbon source via rapid thermal annealing," *Journal of Raman Specroscopy*, vol. 50, no. 11, pp. 1630–1641, 2019.

[51] S. Muhammad Hafiz, R. Ritikos, T. J. Whitcher et al., "A practical carbon dioxide gas sensor using room-temperature hydrogen plasma reduced graphene oxide," *Sensors and Actuators B: Chemical*, vol. 193, pp. 692–700, 2014.

[52] F. T. Johra, J.-W. Lee, and W.-G. Jung, "Facile and safe graphene preparation on solution based platform," *Journal of Industrial and Engineering Chemistry*, vol. 20, no. 5, pp. 2883–2887, 2014.

[53] B. Ma, R. D. Rodriguez, A. Ruban, S. Pavlov, and E. Sheremet, "The correlation between electrical conductivity and second-order Raman modes of laser-reduced graphene oxide," *Physical Chemistry Chemical Physics*, vol. 21, no. 19, pp. 10125–10134, 2019.

[54] T. Kuila, S. Bose, A. K. Mishra, P. Khanra, N. H. Kim, and J. H. Lee, "Chemical functionalization of graphene and its applications," *Progress in Materials Science*, vol. 57, no. 7, pp. 1061–1105, 2012.

[55] R. Sitko, E. Turek, B. Zawisza et al., "Adsorption of divalent metal ions from aqueous solutions using graphene oxide," *Dalton Transactions*, vol. 42, no. 16, pp. 5682–5689, 2013.

[56] X. Ren, J. Li, X. Tan, and X. Wang, "Comparative study of graphene oxide, activated carbon and carbon nanotubes as adsorbents for copper decontamination," *Dalton Transactions*, vol. 42, no. 15, pp. 5266–5274, 2013.

[57] X. Zhang, J. Zhou, H. Song, C. Liu, S. Zhang, and X. Chen, "A reversible transformation of functional groups in graphene oxide with loading and unloading of metal compounds," *Carbon*, vol. 99, pp. 370–374, 2016.

[58] L. S. Čerović, S. K. Milonjić, M. B. Todorović et al., "Point of zero charge of different carbides," *Colloids and Surfaces A: Physicochemical and Engineering Aspects*, vol. 297, no. 1-3, pp. 1–6, 2007.

[59] G. Zhao, J. Li, X. Ren, C. Chen, and X. Wang, "Few-layered graphene oxide nanosheets as superior sorbents for heavy metal ion pollution management," *Environmental Science & Technology*, vol. 45, no. 24, pp. 10454–10462, 2011.

[60] A. Kumar and C. K. Dixit, "Methods for characterization of nanoparticles," in *Advances in Nanomedicine for the Delivery of Therapeutic Nucleic Acids*, pp. 43–58, Elsevier, 2017.

[61] I. Chowdhury, M. C. Duch, N. D. Mansukhani, M. C. Hersam, and D. Bouchard, "Colloidal properties and stability of graphene oxide nanomaterials in the aquatic environment," *Environmental Science & Technology*, vol. 47, no. 12, pp. 6288–6296, 2013.

[62] R. C. Espinoza, U. Sierra-Gómez, C. M. López et al., "Zwitterion-decorated graphene oxide nanosheets with aliphatic amino acids under specific pH conditions," *Applied Surface Science*, vol. 555, p. 149723, 2021.

[63] T.-Y. Lin and D.-H. Chen, "One-step green synthesis of arginine-capped iron oxide/reduced graphene oxide nanocomposite and its use for acid dye removal," *RSC Advances*, vol. 4, no. 56, pp. 29357–29364, 2014.

[64] S. Kim, S. Zhou, Y. Hu et al., "Room-temperature metastability of multilayer graphene oxide films," *Nature Materials*, vol. 11, no. 6, pp. 544–549, 2012.

[65] B. D. Holt, A. M. Arnold, and S. A. Sydlik, "In it for the long haul: the cytocompatibility of aged graphene oxide and its degradation products," *Advanced Healthcare Materials*, vol. 5, no. 23, pp. 3056–3066, 2016.

[66] A. M. Dimiev, L. B. Alemany, and J. M. Tour, "Graphene Oxide. Origin of acidity, its instability in water, and a new dynamic structural model," *ACS Nano*, vol. 7, no. 1, pp. 576–588, 2013.

[67] J. A. Menéndez, M. J. Illán-Gómez, C. A. L. y León, and L. R. Radovic, "On the difference between the isoelectric point and the point of zero charge of carbons," *Carbon*, vol. 33, no. 11, pp. 1655–1657, 1995.

[68] T. Preocanin and N. Kallay, "Point of zero charge and surface charge density of TiO_2 in aqueous electrolyte solution as obtained by potentiometric mass titration," *Croatica Chemica Acta*, vol. 79, pp. 95–106, 2006.

[69] M. Alvarez-Silva, M. Mirnezami, A. Uribe-Salas, and J. A. Finch, "Point of zero charge, isoelectric point and aggregation of phyllosilicate minerals," *Canadian Metallurgical Quarterly*, vol. 49, no. 4, pp. 405–410, 2010.

[70] J. J. Gulicovski, L. S. Čerović, and S. K. Milonjić, "Point of zero charge and isoelectric point of alumina," *Materials and Manufacturing Processes*, vol. 23, no. 6, pp. 615–619, 2008.

[71] T. Mahmood, M. T. Saddique, A. Naeem, P. Westerhoff, S. Mustafa, and A. Alum, "Comparison of different methods for the point of zero charge determination of NiO," *Industrial and Engineering Chemistry Research*, vol. 50, no. 17, pp. 10017–10023, 2011.

[72] K. Bourikas, J. Vakros, C. Kordulis, and A. Lycourghiotis, "Potentiometric mass titrations: experimental and theoretical establishment of a new technique for determining the point of zero charge (PZC) of metal (hydr)oxides," *The Journal of Physical Chemistry. B*, vol. 107, no. 35, pp. 9441–9451, 2003.

[73] M. O. Corapcioglu and C. P. Huang, "The surface acidity and characterization of some commercial activated carbons," *Carbon N. Y.*, vol. 25, no. 4, pp. 569–578, 1987.

[74] V. Strelko, D. J. Malik, and M. Streat, "Characterisation of the surface of oxidised carbon adsorbents," *Carbon*, vol. 40, no. 1, pp. 95–104, 2002.

[75] Y. A. Aydın and N. D. Aksoy, "Adsorption of chromium on chitosan: optimization, kinetics and thermodynamics," *Chemical Engineering Journal*, vol. 151, no. 1-3, pp. 188–194, 2009.

[76] A. A. Inyinbor, F. A. Adekola, and G. A. Olatunji, "Kinetics, isotherms and thermodynamic modeling of liquid phase adsorption of Rhodamine B dye onto *Raphia hookerie* fruit epicarp," *Water Resources and Industry*, vol. 15, pp. 14–27, 2016.

[77] O. Hamdaoui and E. Naffrechoux, "Modeling of adsorption isotherms of phenol and chlorophenols onto granular activated carbon: part I. Two-parameter models and equations allowing determination of thermodynamic parameters," *Journal of Hazardous Materials*, vol. 147, no. 1-2, pp. 381–394, 2007.

[78] A. O. Dada, A. P. Olalekan, A. M. Olatunaya, O. Dada, and F. Langmuir, "Temkin and Dubinin–Radushkevich Isotherms studies of equilibrium sorption of Zn^{2+} unto phosphoric acid modified rice husk," *IOSR Journal of Applied Chemistry*, vol. 3, pp. 38–45, 2012.

[79] K. Y. Foo and B. H. Hameed, "Insights into the modeling of adsorption isotherm systems," *Chemical Engineering Journal*, vol. 156, no. 1, pp. 2–10, 2010.

[80] C. Ng, J. N. Losso, W. E. Marshall, and R. M. Rao, "Freundlich adsorption isotherms of agricultural by-product-based powdered activated carbons in a geosmin-water system," *Bioresource Technology*, vol. 85, no. 2, pp. 131–135, 2002.

[81] G. P. Jeppu and T. P. Clement, "A modified Langmuir-Freundlich isotherm model for simulating pH-dependent adsorption effects," *Journal of Contaminant Hydrology*, vol. 129-130, pp. 46–53, 2012.

[82] R. J. Umpleby, S. C. Baxter, Y. Chen, R. N. Shah, and K. D. Shimizu, "Characterization of molecularly imprinted polymers with the Langmuir–Freundlich isotherm," *Analytical Chemistry*, vol. 73, no. 19, pp. 4584–4591, 2001.

[83] S. Thangavel and G. Venugopal, "Understanding the adsorption property of graphene-oxide with different degrees of oxidation levels," *Powder Technology*, vol. 257, pp. 141–148, 2014.

[84] X. Liu, Y. Huang, S. Duan et al., "Graphene oxides with different oxidation degrees for co(II) ion pollution management," *Chemical Engineering Journal*, vol. 302, pp. 763–772, 2016.

[85] A. C. Reynosa-Martínez, G. N. Tovar, W. R. Gallegos et al., "Effect of the degree of oxidation of graphene oxide on as(III) adsorption," *Journal of Hazardous Materials*, vol. 384, article 121440, 2020.

[86] E. A. El-Sharkaway, R. M. Kamel, I. M. El-Sherbiny, and S. S. Gharib, "Removal of methylene blue from aqueous solutions using polyaniline/graphene oxide or polyaniline/reduced graphene oxide composites," *Environmental Technology*, vol. 41, no. 22, pp. 2854–2862, 2020.

[87] H. Shi, W. Li, L. Zhong, and C. Xu, "Methylene blue adsorption from aqueous solution by magnetic cellulose/graphene oxide composite: equilibrium, kinetics, and thermodynamics," *Industrial and Engineering Chemistry Research*, vol. 53, no. 3, pp. 1108–1118, 2014.

[88] J.-L. Gong, B. Wang, G.-M. Zeng et al., "Removal of cationic dyes from aqueous solution using magnetic multi-wall carbon nanotube nanocomposite as adsorbent," *Journal of Hazardous Materials*, vol. 164, no. 2-3, pp. 1517–1522, 2009.

[89] S. Altenor, B. Carene, E. Emmanuel, J. Lambert, J. J. Ehrhardt, and S. Gaspard, "Adsorption studies of methylene blue and phenol onto vetiver roots activated carbon prepared by chemical activation," *Journal of Hazardous Materials*, vol. 165, no. 1-3, pp. 1029–1039, 2009.

[90] M. Zhao and P. Liu, "Adsorption of methylene blue from aqueous solutions by modified expanded graphite powder," *Desalination*, vol. 249, no. 1, pp. 331–336, 2009.

[91] P. T. Lan Huong, N. Tu, H. Lan et al., "Functional manganese ferrite/graphene oxide nanocomposites: effects of graphene oxide on the adsorption mechanisms of organic MB dye and inorganic As(v) ions from aqueous solution," *RSC Advances*, vol. 8, no. 22, pp. 12376–12389, 2018.

[92] T. Liu, Y. Li, Q. Du et al., "Adsorption of methylene blue from aqueous solution by graphene," *Colloids Surfaces B Biointerfaces*, vol. 90, pp. 197–203, 2012.

[93] Q. Zhang, Y. Gao, Z. Xu, S. Wang, H. Kobayashi, and J. Wang, "The effects of oxygen functional groups on graphene oxide on the efficient adsorption of radioactive iodine," *Materials (Basel).*, vol. 13, no. 24, pp. 1–13, 2020.

[94] Y. Bian, Z. Y. Bian, J. X. Zhang, A. Z. Ding, S. L. Liu, and H. Wang, "Effect of the oxygen-containing functional group of graphene oxide on the aqueous cadmium ions removal," *Applied Surface Science*, vol. 329, pp. 269–275, 2015.

[95] S. Bai, X. Shen, X. Zhong et al., "One-pot solvothermal preparation of magnetic reduced graphene oxide-ferrite hybrids for organic dye removal," *Carbon*, vol. 50, no. 6, pp. 2337–2346, 2012.

[96] Q. Zhuang, H. Liu, T. Li, and T. Zhao, "Bistability and pH hysteresis of graphene oxide solution in circle acid-base titration," *Chemistry Letters*, vol. 44, no. 4, pp. 454–456, 2015.

[97] A. Rodríguez, J. García, G. Ovejero, and M. Mestanza, "Adsorption of anionic and cationic dyes on activated carbon from aqueous solutions: equilibrium and kinetics," *Journal of Hazardous Materials*, vol. 172, no. 2-3, pp. 1311–1320, 2009.

[98] H. Kim, S. O. Kang, S. Park, and H. S. Park, "Adsorption isotherms and kinetics of cationic and anionic dyes on three-dimensional reduced graphene oxide macrostructure," *Journal of Industrial and Engineering Chemistry*, vol. 21, pp. 1191–1196, 2015.

[99] K. Krishnamoorthy, R. Mohan, and S.-J. Kim, "Graphene oxide as a photocatalytic material," *Applied Physics Letters*, vol. 98, no. 24, article 244101, 2011.

[100] S. Liu, S. Li, H. Zhang, L. Wu, L. Sun, and J. Ma, "Removal of uranium(VI) from aqueous solution using graphene oxide and its amine-functionalized composite," *Journal of Radioanalytical and Nuclear Chemistry*, vol. 309, pp. 1–8, 2015.

[101] S. Guo, G. Zhang, Y. Guo, and J. C. Yu, "Graphene oxide-Fe_2O_3 hybrid material as highly efficient heterogeneous catalyst for degradation of organic contaminants," *Carbon*, vol. 60, pp. 437–444, 2013.

[102] O. V. Ovchinnikov, A. V. Evtukhova, T. S. Kondratenko, M. S. Smirnov, V. Y. Khokhlov, and O. V. Erina, "Manifestation of intermolecular interactions in FTIR spectra of methylene blue molecules," *Vibrational Spectroscopy*, vol. 86, pp. 181–189, 2016.

[103] Sílvia H. de Araujo Nicolai, P. R. P. Rodrigues, S. M. L. Agostinho, and J. C. Rubim, "Electrochemical and spectroelectrochemical (SERS) studies of the reduction of methylene blue on a silver electrode," *Journal of Electroanalytical Chemistry*, vol. 527, no. 1-2, pp. 103–111, 2002.

[104] K. Imamura, E. Ikeda, T. Nagayasu, T. Sakiyama, and K. Nakanishi, "Adsorption behavior of methylene blue and its congeners on a stainless steel surface," *Journal of Colloid and Interface Science*, vol. 245, no. 1, pp. 50–57, 2002.

[105] J. Bujdák, N. Iyi, Y. Kaneko, and R. Sasai, "Molecular orientation of methylene blue cations adsorbed on clay surfaces," *Clay Minerals*, vol. 38, no. 4, pp. 561–572, 2003.

[106] J. Ederer, P. Janoš, P. Ecorchard et al., "Determination of amino groups on functionalized graphene oxide for polyurethane nanomaterials: XPS quantitation vs. functional speciation," *RSC Advances*, vol. 7, no. 21, pp. 12464–12473, 2017.